iScience

CellPress
OPEN ACCESS

Article

SPECT/CT imaging reveals CNS-wide modulation of glymphatic cerebrospinal fluid flow by systemic hypertonic saline

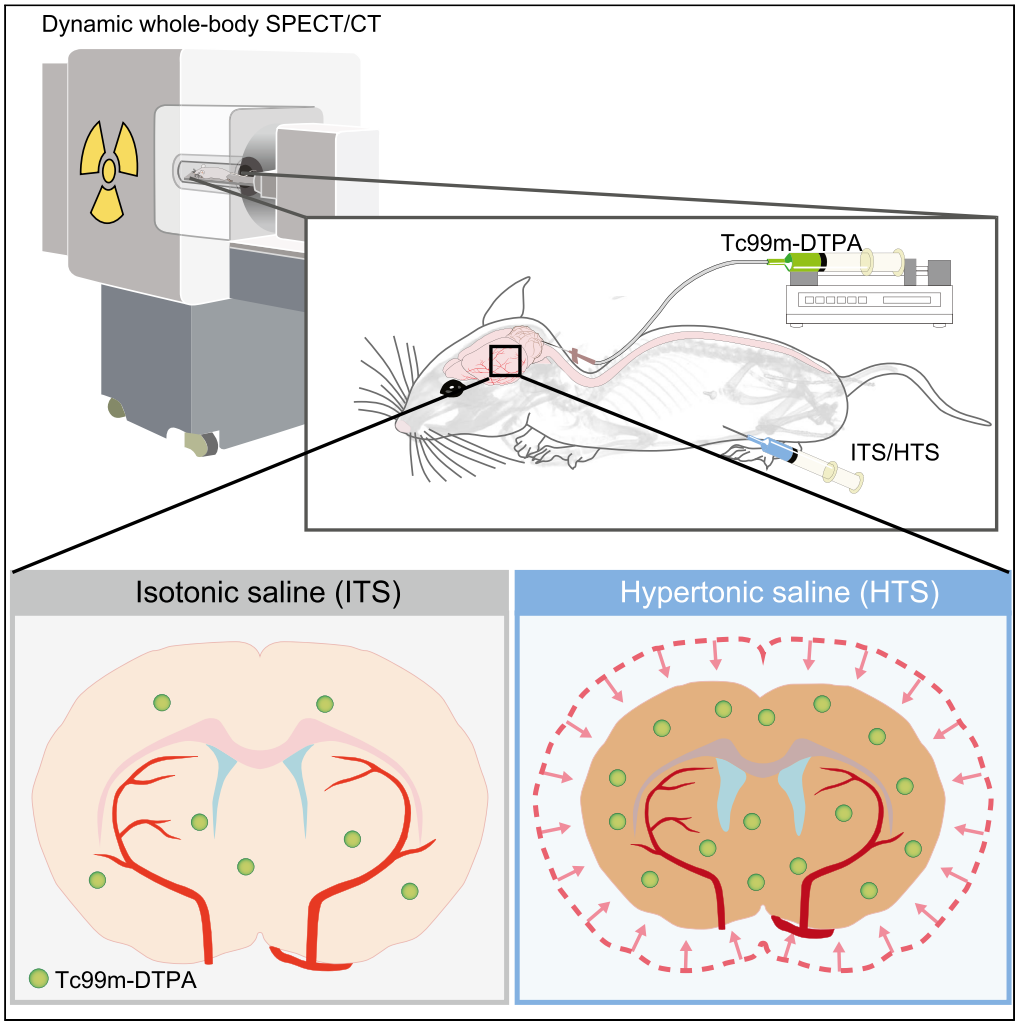

Tuomas O. Lilius, Marko Rosenholm, Laura Klinger, ..., Malthe Skytte Nordentoft Nielsen, Tomi Rantamäki, Maiken Nedergaard

maiken_nedergaard@urmc.rochester.edu

Highlights

We established a SPECT/CT platform for imaging glymphatic drug delivery *in vivo*

Hypertonic saline (HTS) elevates intracranial availability of CSF-infused ^{99m}Tc-DTPA

HTS triples the availability of ^{99m}Tc-DTPA in several deep brain regions

HTS has negligible effects on clearance of intrastriatally infused DTPA

Lilius et al., iScience *25*, 105250
October 21, 2022
https://doi.org/10.1016/j.isci.2022.105250

iScience

CellPress
OPEN ACCESS

Article

SPECT/CT imaging reveals CNS-wide modulation of glymphatic cerebrospinal fluid flow by systemic hypertonic saline

Tuomas O. Lilius,[1,2,3,4,10] Marko Rosenholm,[1,2,10] Laura Klinger,[1] Kristian Nygaard Mortensen,[1] Björn Sigurdsson,[1] Frida Lind-Holm Mogensen,[1,5,6] Natalie L. Hauglund,[1] Malthe Skytte Nordentoft Nielsen,[1] Tomi Rantamäki,[7,8] and Maiken Nedergaard[1,9,11,*]

SUMMARY

Intrathecal administration enables central nervous system delivery of drugs that do not bypass the blood-brain barrier. Systemic administration of hypertonic saline (HTS) enhances delivery of intrathecal therapeutics into the neuropil, but its effect on solute clearance from the brain remains unknown. Here, we developed a dynamic *in vivo* single-photon emission computed tomography (SPECT)/computed tomography (CT) imaging platform to study the effects of HTS on whole-body distribution of the radiolabeled tracer ^{99m}Tc-diethylenetriaminepentaacetic acid (DTPA) administered through intracisternal, intrastriatal, or intravenous route in anesthetized rats. Co-administration of systemic HTS increased intracranial exposure to intracisternal ^{99m}Tc-DTPA by ~80% during imaging. In contrast, HTS had minimal effects on brain clearance of intrastriatal ^{99m}Tc-DTPA. In sum, SPECT/CT imaging presents a valuable approach to study glymphatic drug delivery. Using this methodology, we show that systemic HTS increases intracranial availability of cerebrospinal fluid-administered tracer, but has marginal effects on brain clearance, thus substantiating a simple, yet effective strategy for enhancing intrathecal drug delivery to the brain.

INTRODUCTION

Delivery of drugs to the central nervous system (CNS) is limited by the selective permeability of the blood-brain barrier (BBB), which prevents over 98% of small-molecule drugs from reaching a therapeutically relevant drug concentration in the brain after systemic administration (Banks, 2016; Begley, 2004; Calias et al., 2014; Geary et al., 2015; Pardridge, 2005; Thorne and Frey, 2001). Various delivery strategies aimed at bypassing the BBB have been developed, but their clinical applications remain scarce (Calias et al., 2014; Chen and Liu, 2012; Kariolis et al., 2020; Ullman et al., 2020). An attractive approach for enhanced CNS drug delivery is provided by the recently described brain-wide fluid transport pathway, termed the glymphatic system. The glymphatic system consists of bulk flow of cerebrospinal fluid (CSF) deep into the brain along perivascular spaces (PVS) of pial and penetrating arteries, where it facilitates exchange of CSF and interstitial fluid (ISF) through a fenestrated barrier of astrocytic endfeet and clearance of interstitial solutes (Iliff et al., 2012; Nedergaard, 2013; Xie et al., 2013). Prior methods for imaging the glymphatic pathway in the living brain are efficient for detecting the influx of CSF tracers to the brain parenchyma, but have limited fitness to detect global changes in CSF distribution as well as efflux and elimination of the administered tracer from brain. We thus perceive a need for novel *in vivo* imaging techniques to quantify CNS-wide macromolecule distribution via glymphatic transport.

CSF flow in the periarterial spaces toward the brain parenchyma is facilitated by arterial pulsatility (Mestre et al., 2018), and exchange of CSF with ISF is influenced by brain state (Hablitz et al., 2019; Xie et al., 2013). In addition to physiological factors, certain pharmacological interventions can also enhance CSF influx and promote glymphatic delivery of intrathecally administered agents. This phenomenon has been observed with systemic and intrathecal administration of the α_2-adrenergic agonist dexmedetomidine (Benveniste et al., 2017; Lilius et al., 2019), but even more markedly by transient elevation of plasma osmolarity following systemic administration of hypertonic solutions, such as hypertonic saline (HTS) or mannitol (Pizzo et al.,

[1]Center for Translational Neuromedicine, Faculty of Health and Medical Sciences, University of Copenhagen, Copenhagen, Denmark

[2]Individualized Drug Therapy Research Program, Faculty of Medicine, University of Helsinki, Helsinki, Finland

[3]Department of Pharmacology, Faculty of Medicine, University of Helsinki, Helsinki, Finland

[4]Department of Emergency Medicine and Services, Helsinki University Hospital and University of Helsinki, Helsinki, Finland

[5]Neuro-immunology Group, Department of Cancer Research, Luxembourg Institute of Health, Luxembourg, Luxembourg

[6]Doctoral School of Science and Technology, University of Luxembourg, Esch-sur-Alzette, Luxembourg

[7]Laboratory of Neurotherapeutics, Doctoral Program in Drug Research, Faculty of Pharmacy, University of Helsinki, Helsinki, Finland

[8]SleepWell Research Program, Faculty of Medicine, University of Helsinki, Helsinki, Finland

[9]Center for Translational Neuromedicine, Department of Neurosurgery, University of Rochester Medical Center, 601 Elmwood Avenue, Box 645, Rochester, NY 14642, USA

[10]These authors contributed equally

[11]Lead contact

*Correspondence: maiken_nedergaard@urmc.rochester.edu

https://doi.org/10.1016/j.isci.2022.105250

2018; Plog et al., 2018). More specifically, systemic HTS induced a 5-fold increase in parenchymal delivery of intrathecal amyloid-β (Aβ) antibody (Plog et al., 2018). This enhancement of CSF influx was driven by efflux of fluid from CNS into the hyperosmolar plasma following along the osmotic gradient, which in turn accelerated periarterial influx of CSF along the altered pressure gradient within the rigid cavity of the skull. In another study, intrathecal mannitol dose dependently increased the perivascular access of a co-infused full-length IgG antibody (Pizzo et al., 2018). These findings suggest that hypertonic solutions could be suitable as an intervention to enhance brain delivery of intrathecally administered drugs. HTS has been in clinical use for over a century, with a main application in osmotherapy for decreasing elevated intracranial pressure of life-threatening cerebral edema (Todd, 2013). Hyperosmotic treatment is well tolerated and readily available in the clinic without any requirement for concurrent anesthesia or sedation.

Here, we established an *in vivo* imaging platform based on dynamic single-photon emission computed tomography/computed tomography (SPECT/CT) that enables quantitative whole-body imaging of radiolabeled tracer distribution in rats. Using this platform, we tested the hypothesis that increasing plasma osmolarity would enhance the parenchymal delivery of the low-molecular-weight tracer ^{99m}Tc-diethylenetriaminepentaacetic acid (DTPA, 489 Da) administered through the intracisternal route in anesthetized rats. Since the effects of HTS on glymphatic efflux are not known, we also addressed distribution and brain clearance of intrastriatal ^{99m}Tc-DTPA. In addition, we used magnetic resonance imaging (MRI) to quantify HTS-induced changes in brain and CSF volumes and osmolality measurements of blood and CSF to determine the physiological mechanisms underlying HTS influence on fluid flow. Furthermore, we performed a battery of behavioral tests to assess the safety of the used HTS dose in awake rats.

RESULTS

Systemic HTS dramatically increases intracranial availability of intracisternally infused ^{99m}Tc-DTPA

To assess the global effects of systemic HTS on intracisternally infused tracer distribution, we imaged anesthetized rats with SPECT/CT for 220 min. During the first 20 min the animals received an intracisternal infusion of ^{99m}Tc-DTPA (1.6 μL/min) immediately followed by administration of either HTS (1 M NaCl, 20 mL/kg, 40 mOsm/kg, intraperitoneally [i.p.], n = 7) or isotonic saline (ITS, 0.154 M NaCl, control group, 20 mL/kg, 6.16 mOsm/kg, i.p., n = 7) (Figure 1A). The HTS dose was selected based on a previous report, where similar dosing evoked an increase in plasma Na^+ concentration comparable to that in clinical osmotherapy (Järvelä et al., 2003; Plog et al., 2018; Tølløfsrud et al., 1998). Neither the monitored basic physiological parameters nor the infused radioactivity dose differed between treatment groups (Figure S1). Whole-body SPECT image frames were acquired at 10-min intervals and reconstructed. The decay-corrected radioactivity concentration was quantified in regions of interest (ROIs) defined in the CT anatomic reference images acquired directly after the SPECT scan (Figures 1B and 1C, Video S1). ^{99m}Tc-DTPA activity in the imaging field of view (FOV) remained stable throughout the entire 220-min acquisition, confirming that the total infused activity remained within the FOV (Figure 1D). As determined by area under the time-activity curve ($AUC_{0\text{-}220}$), the detected tracer activity in the intracranial region was ~80% higher in animals receiving HTS (Figure 1E, $p < 0.001$, unpaired Student's t test). The treatment with HTS also tripled tracer activity in the striatum (Figure 1F, $p < 0.001$, unpaired Student's t test) and several other brain regions, with the largest increase (5-fold) in the cortical volume of interest ($p < 0.001$, unpaired Student's t test), demonstrating that tracer entry into widespread brain structures was dramatically enhanced by HTS (Figures S2A–S2D). In contrast, spinal radioactivity was lower in the HTS group (Figure 1G, $p < 0.01$, unpaired Student's t test). Outside CNS, the sum of total radioactivity was significantly lower after HTS administration (Figure 1H, $p < 0.05$, unpaired Student's t test). Correspondingly, the HTS group exhibited significantly lower tracer radioactivity in several CSF efflux regions, including the nasal cavity ($p < 0.001$, unpaired Student's t test), deep cervical lymph nodes (DCLN, $p < 0.05$, unpaired Student's t test), and mandibular lymph nodes (MLN, $p < 0.05$, unpaired Student's t test) (Figures 1I, S2E, and S2F). In accordance with the increased intracranial availability, systemic excretion of the tracer was significantly reduced after HTS administration, as indicated by significantly decreased radioactivity in heart, ($p < 0.05$, unpaired Student's t test) and a small, but non-significant activity decrease in the kidneys (Figures 1J and 1K). DTPA is eliminated exclusively through the kidney, without active transport in the tubules (Taylor, 2014). After 220 min, approximately 40% of the administered radioactivity was found in urine in the control group, whereas only 20% was excreted to urine in the group treated with HTS (Figure 1L, $p < 0.001$, unpaired Student's t test). Overall, HTS caused a substantial increase in brain availability of intracisternally administered ^{99m}Tc-DTPA, whereas tracer activity in regions relevant for CSF efflux and elimination was higher in the control group (Figure 1M).

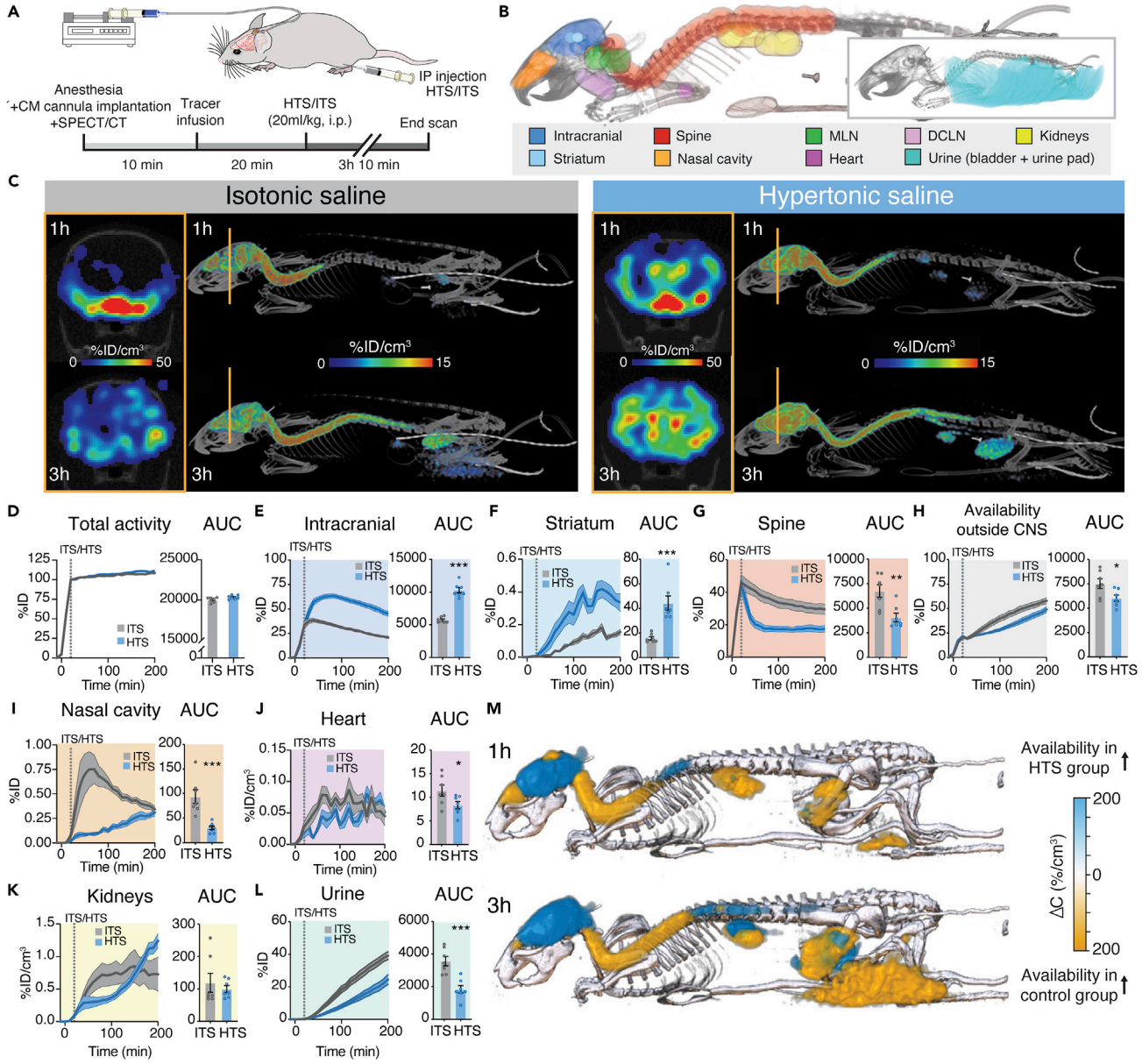

Figure 1. Systemic HTS significantly increases cerebral influx of intrathecal ^{99m}Tc-DTPA

(A) Experimental timeline.

(B) Regions of interest (ROIs) overlain on a rat CT image.

(C) Representative SPECT/CT images and coronal slices showing ^{99m}Tc-DTPA distribution at selected time points of the scan.

(D) Decay-corrected time-activity analysis of total tracer activity in the imaging field of view.

(E–G) ^{99m}Tc-DTPA distribution in CNS regions. HTS treatment increases intracranial and striatal availability of cisterna magna-infused tracer, while decreasing its distribution to spinal CSF.

(H) ^{99m}Tc-DTPA has lower clearance outside the CNS after HTS administration.

(I–L) HTS slows tracer clearance from the brain and body, as demonstrated by decreased radioactivity in nasal cavity, heart, and urine.

(M) Difference in group-wise averaged ^{99m}Tc-DTPA radioactivity between treatment groups projected on a rat CT image. The data are presented as mean ± SEM; n = 7 rats/group. ***p < 0.001, **p < 0.01, *p < 0.05, unpaired Student's t test. ITS, isotonic saline; HTS, hypertonic saline; ID, infused dose; DCLN, deep cervical lymph nodes; MLN, mandibular lymph nodes.

The observations thereby support the hypothesis that HTS co-administration may serve to improve brain delivery of an intrathecally administered tracer, in this case tripling the activity of ^{99m}Tc-DTPA in the striatum.

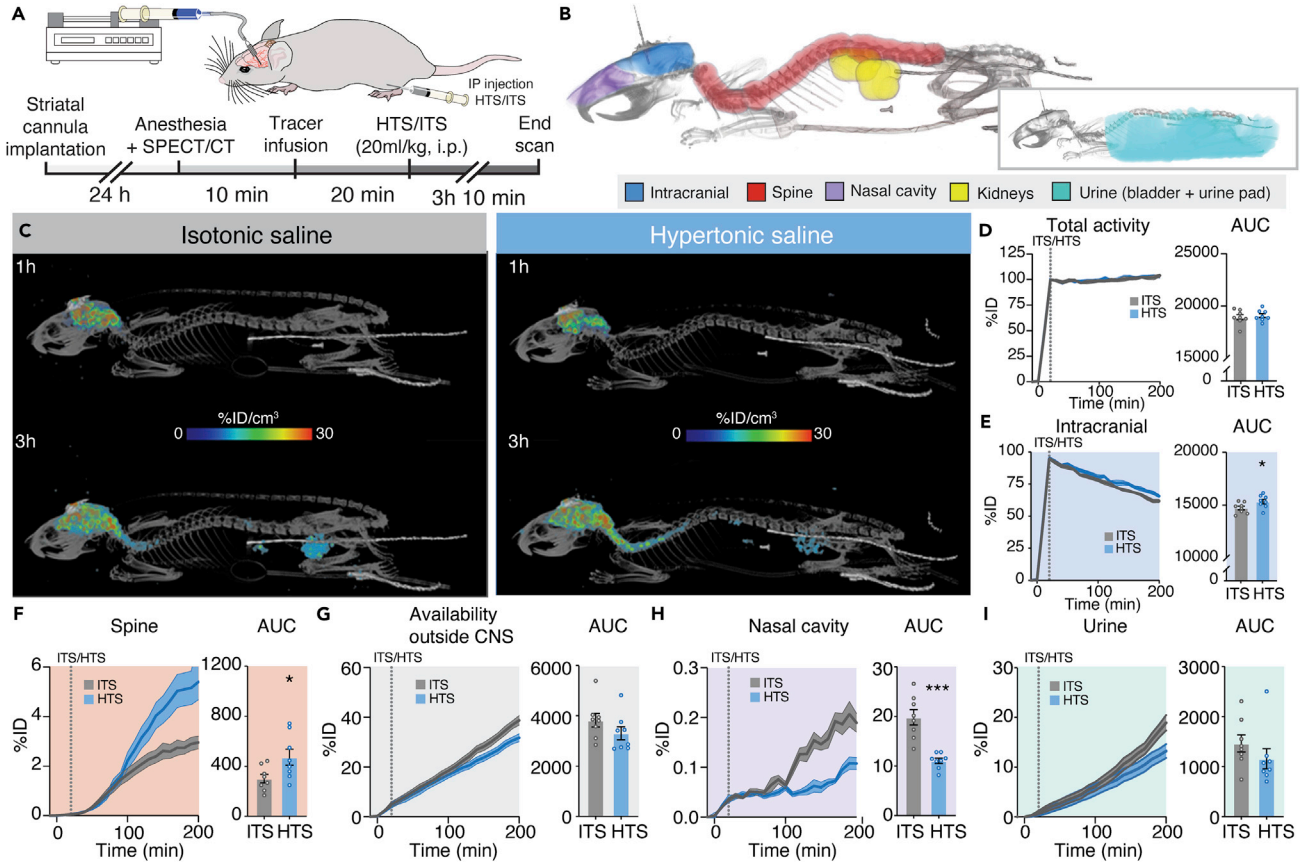

Figure 2. Minimal effects of HTS on clearance dynamics of intrastriatally infused ^{99m}Tc-DTPA

(A) Experimental timeline.

(B) Regions of interest (ROIs) overlain on the rat CT image.

(C) Representative SPECT/CT fusion image of ^{99m}Tc-DTPA distribution at selected time points of the scan.

(D) Decay-corrected time-activity analysis of total tracer radioactivity concentration in the imaging field of view.

(E–I) ^{99m}Tc-DTPA distribution in the defined ROIs. Systemic HTS increases intracranial availability of intrastriatally infused ^{99m}Tc-DTPA, decreases the radioactivity in the nasal cavity, and directs the efflux toward the spinal compartment. Effects of HTS remained minimal on summed ^{99m}Tc-DTPA activity in peripheral tissues and in the urine. The data are presented as mean ± SEM; n = 8 rats/group. ***p < 0.001, *p < 0.05, unpaired Student's t test. ITS, isotonic saline; HTS, hypertonic saline; ID, infused dose.

HTS treatment has minimal effect on clearance of intrastriatally infused ^{99m}Tc-DTPA

Clearance of ISF and solutes is an essential functional aspect of the glymphatic system (Iliff et al., 2012). However, the effects of HTS on glymphatic solute clearance have not been previously characterized. To test whether plasma hyperosmolality also impacts tracer clearance from the neuropil, we measured the effect of systemic HTS on tracer distribution in another cohort of rats that received ^{99m}Tc-DTPA via a chronically implanted cannula in the striatum (infused at a rate of 0.2 μL/min over 20 min, n = 8/group) during whole-body SPECT/CT imaging for 220 min (Figures 2A–2C). Quantitation of total tracer activity in the whole body and urine pad confirmed that we were able to recover the entire tracer radioactivity throughout the scan (Figure 2D). Interestingly, HTS co-administration did not increase clearance of intrastriatally infused ^{99m}Tc-DTPA from the brain; in contrast, intracranial radioactivity as determined by $AUC_{0\text{-}220}$ was slightly increased after HTS (Figure 2E, Video S2, $p < 0.05$, unpaired Student's t test). This result may be attributed to the slow clearance of radioactivity from the intracranial space in both groups, with more than 50% of the infused dose remaining in the intracranial region after the 220-min scan. HTS decreased ^{99m}Tc-DTPA radioactivity in the nasal cavity ($p < 0.001$, unpaired Student's t test), but increased spinal concentration ($p < 0.05$, unpaired Student's t test), indicating that HTS induced a switch in the direction of net tracer efflux from the olfactory region to the spinal canal (Figures 2F and 2H). However, the tracer concentration in these regions remained low (<10 %ID) throughout the scan. HTS had no effect on summed ^{99m}Tc-DTPA activity outside the CNS regions (Figure 2G). A negligible fraction of the infused activity was

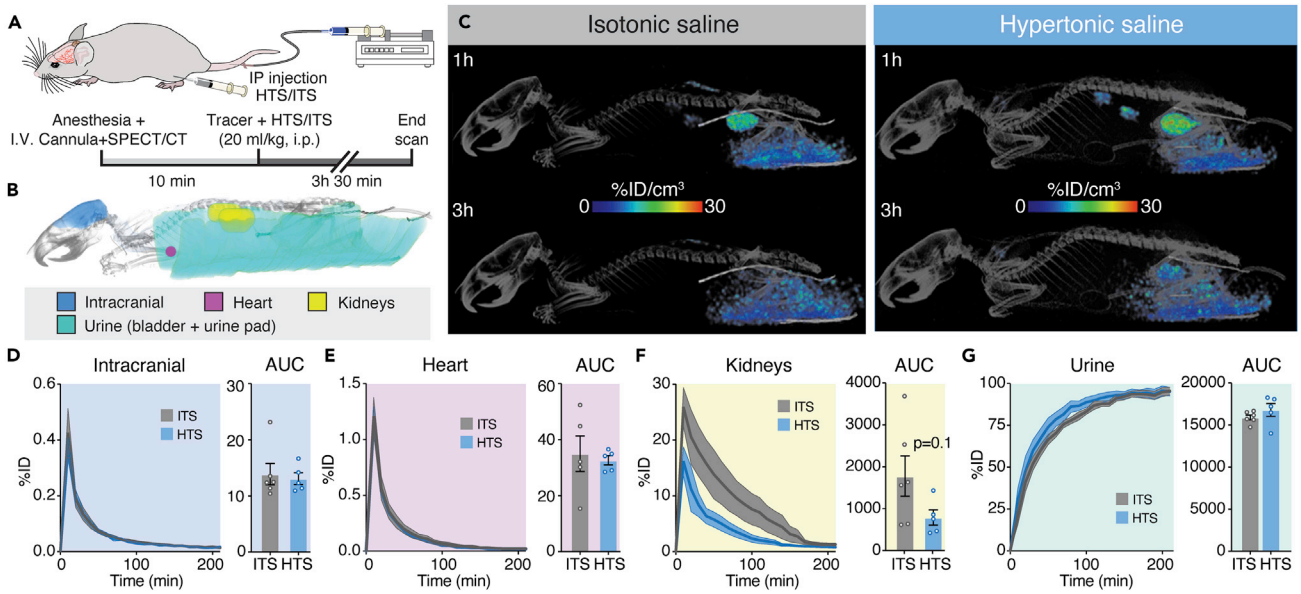

Figure 3. HTS does not influence brain availability or renal elimination of intravenously administered ^{99m}Tc-DTPA

(A) Experimental timeline.

(B) Representative SPECT/CT image of ^{99m}Tc-DTPA distribution at selected time points of the scan.

(C) Regions of interest (ROIs) overlapped to the rat CT image.

(D–G) Decay-corrected time-activity analysis of ^{99m}Tc-DTPA in the defined ROIs. HTS causes negligible effects on the renal elimination of the tracer. The data are presented as mean ± SEM; n = 6 (ITS group), n = 5 (HTS group). Unpaired Student's t test.

observed in lymph node (DCLN, MLN) and heart regions in each imaging frame, detection of which was limited by the small infusion volume and radioactivity used in the striatal infusion (Figure S1B). No differences between treatment groups were observed in these regions (data not shown). Also, the low molecular weight of ^{99m}Tc-DTPA (489 Da) likely disfavored tracer accumulation in the lymph nodes. Elimination of ^{99m}Tc-DTPA in the urine was unaffected by HTS administration (Figure 2I). Overall, HTS co-administration had only minor effects on the clearance of intrastriatally infused ^{99m}Tc-DTPA, which stands in stark contrast to its remarkable enhancement of tracer influx from the subarachnoid CSF.

Intravenous ^{99m}Tc-DTPA administration shows that HTS does not influence BBB permeability or glomerular filtration

To determine whether the observed effects of HTS on ^{99m}Tc-DTPA distribution were influenced by potential HTS-induced alterations in BBB permeability or by altered glomerular filtration rate, we studied the distribution of intravenously administered tracer (200-µL bolus) in an additional cohort of rats after systemic ITS (n = 6) or HTS (n = 5) administration (Figures 3A–3C). The distribution kinetics in the intracranial region and heart ROI were identical between the ITS and HTS groups, indicating that ^{99m}Tc-DTPA did not access parenchyma in either group and that HTS does not increase the BBB permeability to ^{99m}Tc-DTPA (Figures 3D and 3E). HTS administration caused a slight, but non-significant decrease in average tracer radioactivity in the kidneys (Figure 3F, p = 0.1, unpaired Student's t test). However, HTS did not affect ^{99m}Tc-DTPA activity in the urine, indicating that HTS administration may increase the rate of tracer transfer from kidneys to urine (Figure 3G, Video S3). Overall, the results suggest that the decreased elimination of ^{99m}Tc-DTPA to urine observed in intracisternal and intrastriatal experiments is not mediated by effects of HTS on tracer excretion.

Systemic HTS causes a transient decrease in locomotion

In clinical use, HTS administration causes rapid dehydration of the brain, which is reportedly associated with short-lasting headache, heat sensations, and a small risk of pontine demyelination in hyponatremic patients undergoing rapid correction of plasma osmolarity (Himi et al., 1996; Järvelä et al., 2003; Kleinschmidt-DeMasters and Norenberg, 1981; Tølløfsrud et al., 1998). No other serious complications of HTS have been reported. To investigate the behavioral safety aspects of HTS, we next exposed rats to a battery of

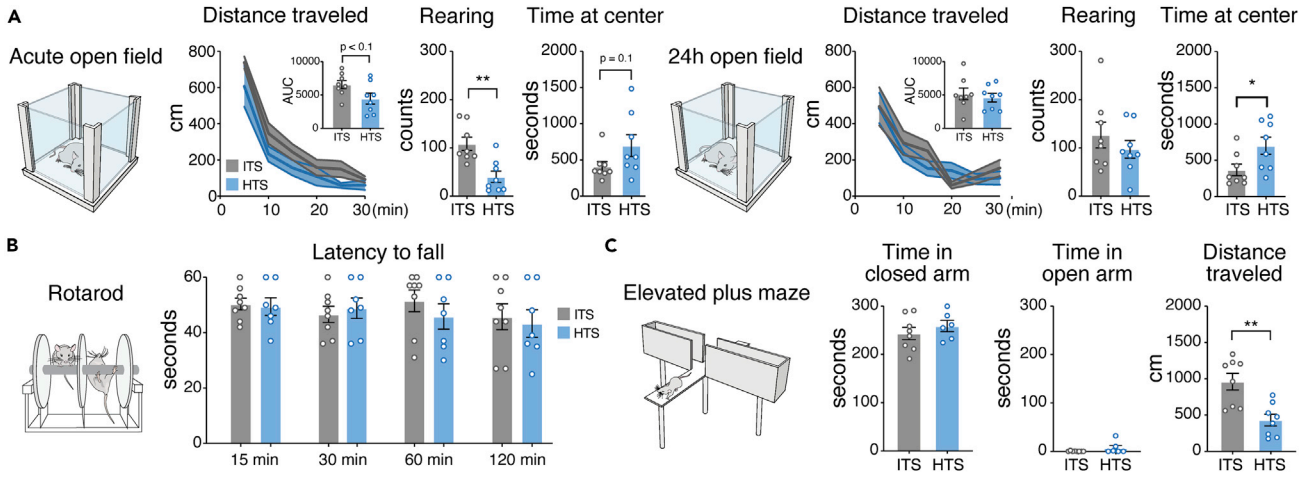

Figure 4. Systemic HTS administration provokes a transient reduction in locomotion

(A) HTS-administered rats express hypolocomotion and decreased rearing behavior in a 30-min open field test performed immediately after HTS administration. The effects of HTS on locomotion and rearing in an open field test had normalized at 24 h after the treatment, but the HTS group persisted in showing increased time at the center of the arena.

(B) HTS had no effects on the latency to fall from the rotarod platform.

(C) In an elevated plus maze test performed immediately after HTS treatment, rats showed a decrease in locomotor activity, but no change in time spent at open or closed compartments of the maze. The data are presented as mean ± SEM; n = 8 rats/group. **p < 0.01, *p < 0.05, unpaired Student's t test. ITS, isotonic saline; HTS, hypertonic saline.

acute behavioral experiments immediately after administering HTS or ITS (n = 8/group). The behavioral tests included open field, rotarod, and elevated plus maze (EPM) tests. The open field test was repeated 24 h after treatments.

In the open field test, HTS caused a transient reduction in locomotion and decreased rearing behavior (Figure 4A). Both locomotion and rearing had returned to normal 24 h later. The HTS and ITS groups responded with similar within-trial and inter-trial habituation to a novel environment. However, HTS-treated rats spent more time at the center of the open field arena when compared with the control group. This effect was still evident in open field test performed 24 h after administrations. The rotarod test, however, revealed no differences between the treatment groups, indicating that motor coordination was unaffected by HTS treatment, and therefore not responsible for the decreased locomotion observed in the open field (Figure 4B).

In the EPM, HTS-treated animals showed decreased locomotor activity in line with findings in the open field test (Figure 4C). However, there were no major differences between the treatment groups in time spent in the different compartments of the EPM. Overall, the behavioral assessment revealed modest and transient effects of systemic HTS. Thus, we identified no major behavioral safety issues for the dose of HTS administered.

Systemic HTS decreases brain volume and increases CSF volume and osmolality

To examine the mechanism causing increased glymphatic influx after systemic HTS, we acquired high-resolution T2-weighted magnetic resonance (MR) images before and after systemic HTS injection (n = 4). We observed drastic dilation of large surface veins and superior sagittal sinus after the treatment, with little or no dilation of surface arteries (Figure 5A). The ventricular system and CSF-filled subarachnoid space surrounding the brain dilated visibly, whereas pial periarterial spaces were not visibly affected (Figure 5A). Quantitation showed that the CSF volume increased on average by 4.4% of the intracranial space volume, with an equal decrease in brain tissue volume (Figures 5B and 5C, $p < 0.01$, unpaired Student's t test). To examine the HTS-induced changes in plasma and CSF osmolality over time, we collected blood and CSF samples from animals 30 and 120 min after systemic HTS/ITS administration (n = 4/group). HTS significantly increased plasma and CSF osmolality at both time points (Figures 5D–5F). The increase in plasma osmolality was reflected by a similar increase in plasma sodium concentration. Overall, the results indicate an osmotically driven fluid movement that may explain the increased access of our low-molecular-weight CSF tracer into the brain.

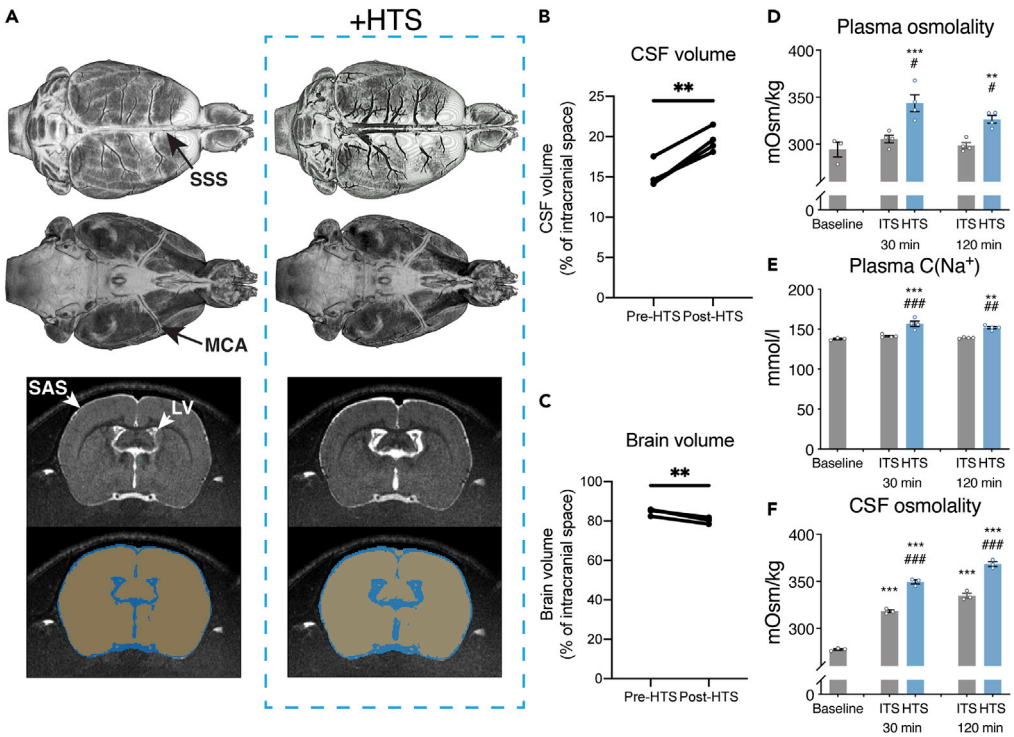

Figure 5. Systemic HTS influences brain fluid compartment volumes and osmolality

(A) Representative MR images of a rat brain before and after systemic HTS administration. HTS dilates the superior sagittal sinus (SSS), dorsal surface veins, and lateral ventricles (LV) visible in coronal slices. The CSF-filled subarachnoid space (SAS) is also enlarged, whereas the effects on arterial blood compartment, such as middle cerebral artery (MCA) size, remain minimal.

(B and C) Quantitation of CSF and brain volumes reveals an increase in CSF volume after systemic HTS administration and an equal decrease in brain volume (n = 4).

(D–F) HTS quickly increases plasma osmolality and sodium concentration, and likewise CSF osmolality. The effects persisted at 120 min after administration. The data are presented as mean ± SEM; n = 3 (baseline group), n = 4 ITS and HTS groups. ***p < 0.001, **p < 0.01, *p < 0.05, unpaired Student's t test (B–C: Pre-HTS versus post-HTS; D–F: Baseline versus HTS). ###p < 0.001, ##p < 0.01, #p < 0.05, unpaired Student's t test (ITS versus HTS). ITS, isotonic saline; HTS, hypertonic saline.

DISCUSSION

Using a dynamic SPECT/CT imaging platform, we revealed that systemic administration of HTS sharply increased intracranial availability of CSF-administered ^{99m}Tc-DTPA in anesthetized rats by ~80%, consequently decreasing its egress from the intracranial space to systemic circulation and slowing its elimination rate from the body. Importantly, HTS administration also increased ^{99m}Tc-DTPA availability in several brain structures: in various deep brain regions after intracisternal infusion it was increased 3-fold, whereas in cortical regions near the dorsal surface of the brain the tracer availability increased 5-fold. HTS did not affect renal elimination of intravenously administered ^{99m}Tc-DTPA, indicating that the decreased tracer elimination observed after intracisternal infusion arises from decreased ^{99m}Tc-DTPA egress from the brain to systemic circulation. Previous studies have shown that systemic administration of hyperosmotic solutions enhances parenchymal distribution of intrathecally administered Aβ-targeted antibody (~100 kDa) and full-length IgG-sized antibody (150 kDa) (Pizzo et al., 2018; Plog et al., 2018). We show here that a similar transient elevation of plasma osmolality enhanced brain delivery of the low-molecular-weight tracer ^{99m}Tc-DTPA. Equally important in this study is the introduction of a dynamic *in vivo* imaging platform that enables quantitation of whole CNS distribution and total clearance of radiolabeled tracer delivered systemically, intrathecally, or into the brain. The data presented in this study strongly support the idea that plasma hyperosmolality-driven CSF influx can be harnessed to improve delivery of intrathecal therapeutics to the CNS.

Prior *in vivo* studies have examined the glymphatic system via 2-photon microscopy (Iliff et al., 2012; Mestre et al., 2018, 2020; Xie et al., 2013), transcranial macroscopic imaging (Plog et al., 2018), and

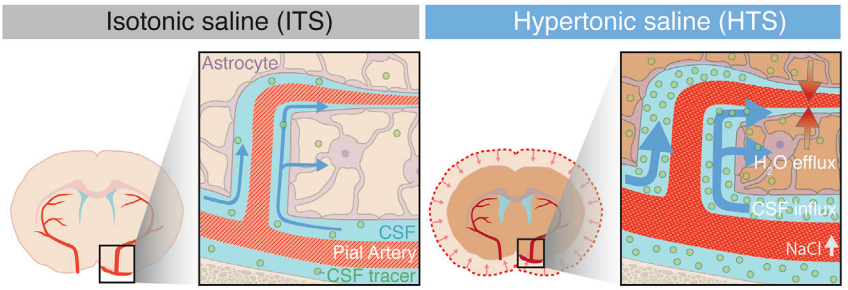

Figure 6. Mechanism of action for the increase in CSF influx driven by plasma hyperosmolality

Increased plasma osmolality draws fluid from the parenchyma into blood, thus decreasing brain volume. The consequent decrease in interstitial pressure facilitates the perivascular influx of CSF into the brain, following along the pressure gradient.

contrast-enhanced MRI (Benveniste et al., 2021; Iliff et al., 2013; Stanton et al., 2021) to visualize CSF tracer flow. Although these techniques provide high spatial detail about tracer distribution within the skull, they are limited in their FOV, and therefore in their capacity to quantify tracer clearance kinetics and distribution in the whole body of the experimental animal. Owing to these limitations, there exists only sparse information regarding the impact of neurodegenerative diseases on glymphatic clearance (Rasmussen et al., 2018). The SPECT/CT imaging platform established here has a major advantage in enabling quantitation of the total clearance of the tracer from its site of injection, as well as tracer distribution throughout the body and its subsequent elimination, enabling kinetic calculations of tracer distribution. In addition, the high sensitivity of SPECT/CT enables the use of smaller tracer volumes than those required in contrast-enhanced MR imaging. The method proved in our hands to be applicable for intracisternal, intrastriatal, and intravenous routes of tracer administration. We were able to detect and account for the total amount of administered tracer throughout the entire 220 min scans. This platform will be useful for imaging and optimizing intrathecal CNS drug delivery and elimination in response to various interventions. In addition, by utilizing the technique in advanced pharmacokinetic modeling, it could be possible to predict the CNS penetrance of an intrathecally administered drug based on its dynamic concentrations in blood and urine samples.

In the clinic, ^{99m}Tc-DTPA is already administered intrathecally in conjunction with SPECT imaging to detect CSF leaks (Lloyd et al., 2008; Novotny et al., 2009) and is a suitable tracer to visualize CSF flow due to its small size, negligible BBB permeability and plasma protein binding, and complete elimination by renal excretion (Hilson et al., 1976; Klopper et al., 1972). Since ^{99m}Tc-DTPA is fully excreted by the kidney and has no active tubular transport, it is routinely used to quantify glomerular filtration rate (Andersen et al., 2019; Rehling et al., 1984, 2001). In contrast to previous studies using large-molecular weight CSF tracers (Pizzo et al., 2018; Plog et al., 2018), ^{99m}Tc-DTPA has a molecular weight of only 489 Da, closely matching that of many intrathecally administered compounds used in the clinic, notably analgesics (e.g., morphine, 285 Da) and chemotherapeutics (e.g., methotrexate 454 Da). As such, ^{99m}Tc-DTPA is an appropriate surrogate for low-molecular-weight pharmaceuticals.

The mechanisms driving increased tracer influx after HTS administration are well established, but the effects of HTS on tracer clearance have remained elusive. The increased influx of CSF tracers after hyperosmolar challenge stems from an increased outflow of water from ISF to plasma across the intact BBB, following along the altered osmotic gradient. Efflux of ISF lowers intracranial pressure (ICP) creating a pressure gradient that drives CSF flow into the parenchyma, carrying CSF-administered compounds along with it (Figure 6) (Plog et al., 2018; Pullen et al., 1987). Although HTS caused a significant decrease in ICP, relative cerebral blood flow and mean arterial blood pressure remained unaltered (Plog et al., 2018). This model is supported by our findings demonstrating a decreased brain volume, accompanied by notable increase in plasma and CSF osmolality after HTS administration. Interestingly, despite these robust physiological effects, we now report that tracer clearance from brain is only modestly affected by HTS. This may be explained by findings reporting that plasma hyperosmolality primarily decreases the brain extracellular volume, whereas intracellular volume remains relatively stable due to rapid ion uptake of the cells after hyperosmolar stress (Cserr et al., 1991; Verbalis, 2010). The reduction in extracellular space volume may increase the physical resistance of the tissue to tracer clearance. In addition, the negligible BBB permeability

of ^{99m}Tc-DTPA (Gilad et al., 2012; Lorberboym et al., 2003) may hinder its clearance to systemic circulation in both iso-osmolar and hyperosmolar conditions.

The findings reported herein present an alternate approach to that reported in our prior study showing that administration of the α_2-adrenergic agonist dexmedetomidine increased CNS delivery of intrathecally administered Aβ antibody (as determined by fluorescence macroscopic imaging) and the low-molecular-weight drugs naloxone and oxycodone (as determined by high-performance liquid chromatography-mass spectrometry analysis of tissue samples) (Lilius et al., 2019). Unlike dexmedetomidine, however, HTS administration does not induce heavy sedation, but rather has been shown to outweigh the suppression of perivascular influx associated with high arousal state (Plog et al., 2018; Xie et al., 2013), thus presenting a notable benefit compared with administration of sedative agents. Systemic HTS is widely used clinically for the treatment of elevated ICP in traumatic brain injury (Bratton et al., 2007). Indeed, HTS is well tolerated in humans, having minimal side effects at doses that maintain the plasma sodium concentration below 150 mM (Himi et al., 1996; Järvelä et al., 2003; Tølløfsrud et al., 1998). The main limitation in the clinical use of HTS is in patients with preexisting hyponatremia, in whom a rapid correction of plasma osmolality has been associated with some risk for central pontine myelinolysis (Kleinschmidt-DeMasters and Norenberg, 1981).

MRI demonstrated a consistent decrease in the brain volume after HTS administration that was accompanied with an equivalent increase in CSF volume. These results together with observed increase in plasma and CSF osmolality support earlier findings that systemic HTS dehydrates the brain by drawing fluid from the brain parenchyma into blood and CSF following along the altered osmotic gradient (Järvelä et al., 2003; Oernbo et al., 2018; Plog et al., 2018). We hypothesized these notable physiological alterations to be reflected in the behavior of the animals, but found the behavioral effects of HTS to be modest, limited to a transient decrease in locomotion. Minor behavioral effects are in line with clinical findings where HTS administration has been well tolerated (Järvelä et al., 2003; Tølløfsrud et al., 1998). Decrease in locomotion may be associated with previously reported transient sedative effects caused by administration of hypertonic solutions (Speck et al., 1988). Overall, our findings indicate no additional concerns for potential negative behavioral effects of systemic HTS administration.

Even though intrathecal drug delivery is a semi-invasive administration method, it has several benefits, including the relatively CNS-specific drug distribution that limits adverse systemic effects, while affording the possibilities to reach therapeutically relevant CNS concentrations with a smaller administered dose, and to obtain extensive delivery of compounds to deep brain structures through the PVS of penetrating arteries. HTS co-administration might be particularly beneficial in intrathecal administration requiring general anesthesia, such as in pediatric patients, where the potential longer administration intervals attained by co-administration of HTS would allow less exposure to anesthetics. In contrast to the intracisternal administration route used in our preclinical study, intrathecal drugs are typically administered into the lumbar subarachnoid space in humans. A prior rodent study showed that lumbar CSF tracers reach the brain parenchyma through the glymphatic pathway, albeit with a significant delay when compared with intracisternal infusion (Yang et al., 2013). That finding is supported by recent clinical studies demonstrating that lumbar CSF tracers attain peak cisternal and intracerebral availability within 4 to 9 hours of administration, depending on the infusion volume (Eide et al., 2021; Ringstad et al., 2018; Verma et al., 2020), indicating that hyperosmotic enhancement of intrathecal drug delivery in the clinic may require that HTS administration is delayed relative to the intrathecal injection. Further support for the therapeutic benefits of HTS-enhanced drug delivery is provided by a recent preclinical study demonstrating an increased antinociceptive effect of intrathecally administered morphine, when administered in conjunction with systemic HTS (Blomqvist et al., 2022). In addition to using lumbar intrathecal administration route, future studies to determine the translational benefits of HTS would also include testing the efficacy of HTS-enhanced delivery of intrathecal large-molecule therapeutics and in treatment of preclinical disease models.

The need for novel drug delivery strategies will likely increase in the future upon the development of large-molecule therapeutics that do not bypass the BBB, including monoclonal antibodies, recombinant proteins, antisense oligonucleotides, and neurotrophic factors. Several innovative technologies to enhance CNS delivery of therapeutics have been developed, including recruitment of transcytosis mechanisms, where therapeutic compounds are labeled with ligands that are actively transported across the BBB,

and the use of nanoparticulate systems or neurotropic viral vectors (Kariolis et al., 2020; Terstappen et al., 2021; Ullman et al., 2020). Despite promising advances, many of these technologies require intricate molecular design and have not yet been established in the clinic. However, since HTS-induced enhancement of CNS drug delivery is limited to intrathecally administered drugs, the BBB-based approaches are important to aid in delivery of CNS drugs through other administration routes. We contend that the HTS administration regimen used in the current study presents a simple, safe, and effective intervention to promote intrathecal drug delivery, thus supporting future studies to test the safety and efficacy of HTS in improving therapeutic response to intrathecal drugs.

Limitations of the study

Limitations of rodent SPECT/CT include the spatial resolution of approximately 0.9 mm (Figure S2H), which disfavors a detailed analysis of tracer distribution between blood, CSF, and ISF compartments within the intracranial space. This necessitates the use of indirect measurements, such as the analysis of a heart ROI to calculate the amount of tracer in systemic circulation. Owing to the low molecular weight and negligible plasma protein binding of ^{99m}Tc-DTPA, we did not find it feasible to measure its concentration and kinetics in some peripheral structures such as the heart and lymph nodes after intraparenchymal delivery, which entails a small infusion volume and consequently low radiochemical dose. For a more detailed spatial distribution analysis, SPECT imaging can be combined with, e.g., *ex vivo* autoradiography of brain slices. CT imaging provides an accurate reference for identification of structures outlined by bone such as the intracranial space and spine, but its limited soft-tissue contrast makes the identification of non-osseous tissues difficult. Whole-body imaging also requires that the rats are anesthetized during imaging, which can introduce confounding effects on glymphatic flow (Hablitz et al., 2019; Xie et al., 2013). Our selection of anesthetic regimen was based on avoiding suppressive effects on glymphatic activity and achieving sufficient level of anesthesia for the whole imaging duration. Ketamine and dexmedetomidine improve the uptake of CSF solutes to the brain, whereas wakefulness or volatile anesthetics such as isoflurane suppress glymphatic CSF flow (Benveniste et al., 2017; Hablitz et al., 2019; Lilius et al., 2019). However, the influx-enhancing effects of plasma hyperosmolality have been shown to be powerful enough to outweigh the suppressive effect of wakefulness and *Aqp4* gene deletion on glymphatic fluid transport and may therefore override the effects of different anesthetic regimens as well, but this remains to be tested (Plog et al., 2018). Finally, the physical half-life (6.0 h) of ^{99m}Tc and rapid renal elimination of ^{99m}Tc-DTPA imposes a practical limitation on the duration of imaging, thus encouraging the use of other radionuclides for assessing slow distribution dynamics.

STAR★METHODS

Detailed methods are provided in the online version of this paper and include the following:

- KEY RESOURCES TABLE
- RESOURCE AVAILABILITY
  - Lead contact
  - Materials availability
  - Data and code availability
- EXPERIMENTAL MODEL AND SUBJECT DETAILS
  - Animals
- METHOD DETAILS
  - Tracers
  - Treatments
  - Tracer administration routes
  - SPECT/CT-imaging
  - SPECT/CT analysis
  - Behavioral tests
  - MR imaging
  - MRI analysis
  - Osmolality and sodium measurements
- QUANTIFICATION AND STATISTICAL ANALYSIS

SUPPLEMENTAL INFORMATION

Supplemental information can be found online at https://doi.org/10.1016/j.isci.2022.105250.

ACKNOWLEDGMENTS

This work was supported by NIH, National Institute of Neurological Disorders and Stroke (R01NS100366 and RF1AG057575, M.N.), U.S. Army Research Office (MURI W911NF1910280, M.N.), Fondation Leducq Transatlantic Networks of Excellence Program (M.N.), The Adelson Foundation (M.N.), EU Horizon 2020 research and innovation programme (grant no. 666881; SVDs@target, M.N. and grant no 798944, GLYMPHARMA, T.O.L.), Novo Nordisk Foundation (M.N.), Lundbeck Foundation (M.N. and M.R.), University of Helsinki Research Funding (T.O.L.), Finnish Medical Foundation (T.O.L.), and Paulo Foundation (T.O.L.). We gratefully acknowledge Mette Møller Jørgensen for radiotracer production; Dan Xue for graphical design and illustrations; Natalie Beschorner, Palle Koch, Ryszard Gomolka, Merja Voutilainen, and Daniel Persson for technical assistance; and Gitte Moos Knudsen and Paul Cumming for expert comments on the manuscript.

AUTHOR CONTRIBUTIONS

Conceptualization: T.O.L., M.N.; Supervision: T.O.L., M.N.; Funding Acquisition: T.O.L., M.N.; Project Administration: T.O.L., M.N., Methodology (imaging): T.O.L., M.N. Methodology (behavior); T.O.L., M.R., T.R.; Resources: T.O.L., T.R., M.N.; Investigation: T.O.L., M.R., L.K., K.N.M., F.L.-H.M., N.L.H.; Formal Analysis: T.O.L., M.R., L.K., K.N.M., B.S., F.L.M., M.S.N.N.; Visualization: M.R., K.N.M., B.S.; Writing – Original Draft: M.R.; Writing – Review & Editing: M.R., T.O.L., M.N.

DECLARATION OF INTERESTS

The authors declare no competing interests.

Received: February 9, 2022
Revised: September 4, 2022
Accepted: September 27, 2022
Published: October 21, 2022

REFERENCES

Andersen, T.B., Jødal, L., Nielsen, N.S., and Petersen, L.J. (2019). Comparison of simultaneous plasma clearance of 99mTc-DTPA and 51Cr-EDTA: can one tracer replace the other? Scand. J. Clin. Lab. Invest. *79*, 463–467. https://doi.org/10.1080/00365513.2019.1658217.

Banks, W.A. (2016). From blood-brain barrier to blood-brain interface: new opportunities for CNS drug delivery. Nat. Rev. Drug Discov. *15*, 275–292. https://doi.org/10.1038/nrd.2015.21.

Begley, D.J. (2004). Delivery of therapeutic agents to the central nervous system: the problems and the possibilities. Pharmacol. Ther. *104*, 29–45. https://doi.org/10.1016/j.pharmthera.2004.08.001.

Benveniste, H., Lee, H., Ding, F., Sun, Q., Al-Bizri, E., Makaryus, R., Probst, S., Nedergaard, M., Stein, E.A., and Lu, H. (2017). Anesthesia with dexmedetomidine and low-dose isoflurane increases solute transport via the glymphatic pathway in rat brain when compared with high-dose isoflurane. Anesthesiology *127*, 976–988. https://doi.org/10.1097/ALN.0000000000001888.

Benveniste, H., Lee, H., Ozturk, B., Chen, X., Koundal, S., Vaska, P., Tannenbaum, A., and Volkow, N.D. (2021). Glymphatic cerebrospinal fluid and solute transport quantified by MRI and PET imaging. Neuroscience *474*, 63–79. https://doi.org/10.1016/j.neuroscience.2020.11.014.

Blomqvist, K.J., Skogster, M.O.B., Kurkela, M.J., Rosenholm, M.P., Ahlström, F.H.G., Airavaara, M.T., Backman, J.T., Rauhala, P.v., Kalso, E.A., and Lilius, T.O. (2022). Systemic hypertonic saline enhances glymphatic spinal cord delivery of lumbar intrathecal morphine. J. Contr. Release *344*, 214–224. https://doi.org/10.1016/j.jconrel.2022.03.022.

Bratton, S.L., Chestnut, R.M., Ghajar, J., Hammond, F.F.M., Harris, O.A., Hartl, R., Manley, G.T., Nemecek, A., Newell, D.W., Rosenthal, G.U.Y., et al. (2007). Guidelines for the management of severe traumatic brain injury. II. Hyperosmolar therapy. J. Neurotrauma *24*, 14–20. https://doi.org/10.1089/neu.2007.9994.

Calias, P., Banks, W.A., Begley, D., Scarpa, M., and Dickson, P. (2014). Intrathecal delivery of protein therapeutics to the brain: a critical reassessment. Pharmacol. Ther. *144*, 114–122. https://doi.org/10.1016/j.pharmthera.2014.05.009.

Chen, Y., and Liu, L. (2012). Modern methods for delivery of drugs across the blood-brain barrier. Adv. Drug Deliv. Rev. *64*, 640–665. https://doi.org/10.1016/j.addr.2011.11.010.

Cserr, H.F., Depasquale, M., Nicholson, C., Patlak, C.S., Pettigrew, K.D., and Rice, M.E. (1991). Extracellular volume decreases while cell volume is maintained by ion uptake in rat brain during acute hypernatremia. J. Physiol. *442*, 277–295.

Eide, P.K., Mariussen, E., Uggerud, H., Pripp, A.H., Lashkarivand, A., Hassel, B., Christensen, H., Hovd, M.H., and Ringstad, G. (2021). Clinical application of intrathecal gadobutrol for assessment of cerebrospinal fluid tracer clearance to blood. JCI Insight *6*, 147063. https://doi.org/10.1172/jci.

Geary, R.S., Norris, D., Yu, R., and Bennett, C.F. (2015). Pharmacokinetics, biodistribution and cell uptake of antisense oligonucleotides. Adv. Drug Deliv. Rev. *87*, 46–51. https://doi.org/10.1016/j.addr.2015.01.008.

Gilad, R., Lampl, Y., Eilam, A., Boaz, M., and Loyberboim, M. (2012). SPECT-DTPA as a tool for evaluating the blood-brain barrier in post-stroke seizures. J. Neurol. *259*, 2041–2044. https://doi.org/10.1007/s00415-012-6445-2.

Hablitz, L.M., Vinitsky, H.S., Sun, Q., Stæger, F.F., Sigurdsson, B., Mortensen, K.N., Lilius, T.O., and Nedergaard, M. (2019). Increased glymphatic influx is correlated with high EEG delta power and low heart rate in mice under anesthesia. Sci. Adv. *5*, 1–8. https://doi.org/10.1126/sciadv.aav5447.

Hilson, A.J.W., Mistry, R.D., and Maisey, M.N. (1976). 99Tcm-DTPA for the measurement of glomerular filtration rate. Br. J. Radiol. *49*, 794–796.

Himi, K., Takemoto, A., Himi, S., Hayasaka, K., Okuhata, Y., Urahashi, S., Tanaka, Y., Hirayama, T., Katayama, Y., Zubair Hossain, M.I., et al. (1996). Heat and pain sensations induced by arterial injection of low-osmolality contrast media: a comparison of patients' discomfort with ionic saline, nonionic glucose, and vasodilator nitrate. Acad. Radiol. *3*, 8214–S217.

Iliff, J.J., Lee, H., Yu, M., Feng, T., Logan, J., Nedergaard, M., and Benveniste, H. (2013). Brain-wide pathway for waste clearance captured by contrast-enhanced MRI. J. Clin. Invest. *123*, 1299–1309. https://doi.org/10.1172/JCI67677.

Iliff, J.J., Wang, M., Liao, Y., Plogg, B.A., Peng, W., Gundersen, G.A., Benveniste, H., Vates, G.E., Deane, R., Goldman, S.A., et al. (2012). A paravascular pathway facilitates CSF flow through the brain parenchyma and the clearance of interstitial solutes, including amyloid β. Sci. Transl. Med. *4*, 147ra111. https://doi.org/10.1126/scitranslmed.3003748.

Järvelä, K., Koskinen, M., and Kööbi, T. (2003). Effects of hypertonic saline (7.5%) on extracellular fluid volumes in healthy volunteers. Anaesthesia *58*, 874–877. https://doi.org/10.1046/j.1365-2044.2003.03335.x.

Kariolis, M.S., Wells, R.C., Getz, J.A., Kwan, W., Mahon, C.S., Tong, R., Kim, D.J., Srivastava, A., Bedard, C., Henne, K.R., et al. (2020). Brain delivery of therapeutic proteins using an Fc fragment blood-brain barrier transport vehicle in mice and monkeys. Sci. Transl. Med. *12*, 1–14. https://doi.org/10.1126/scitranslmed.aay1359.

Kleinschmidt-DeMasters, B.K., and Norenberg, M.D. (1981). Rapid correction of hyponatremia causes demyelination: relation to central pontine myelinolysis. Science *211*, 1068–1070. https://doi.org/10.1038/050458a0.

Klopper, J.F., Hauser, W., Atkins, H.L., Eckelman, W.C., and Richards, P. (1972). Evaluation of 99m Tc-DTPA for the measurement of glomerular filtration rate. J. Nucl. Med. *13*, 107–110.

Lilius, T.O., Blomqvist, K., Hauglund, N.L., Liu, G., Stæger, F.F., Bærentzen, S., Du, T., Ahlström, F., Backman, J.T., Kalso, E.A., et al. (2019). Dexmedetomidine enhances glymphatic brain delivery of intrathecally administered drugs. J. Contr. Release *304*, 29–38. https://doi.org/10.1016/j.jconrel.2019.05.005.

Lloyd, K.M., DelGaudio, J.M., and Hudgins, P.A. (2008). Imaging of skull base cerebrospinal fluid leaks in adults. Radiology *248*, 725–736. https://doi.org/10.1148/radiol.2483070362.

Lorberboym, M., Lampl, Y., and Sadeh, M. (2003). Correlation of 99m Tc-DTPA SPECT of the blood-brain barrier with neurologic outcome after acute stroke. J. Nucl. Med. *44*, 1898–1904.

Mestre, H., Du, T., Sweeney, A.M., Liu, G., Samson, A.J., Peng, W., Mortensen, K.N., Stæger, F.F., Bork, P.A.R., Bashford, L., et al. (2020). Cerebrospinal fluid influx drives acute ischemic tissue swelling. Science *367*, eaax7171. https://doi.org/10.1126/science.aax7171.

Mestre, H., Tithof, J., Du, T., Song, W., Peng, W., Sweeney, A.M., Olveda, G., Thomas, J.H., Nedergaard, M., and Kelley, D.H. (2018). Flow of cerebrospinal fluid is driven by arterial pulsations and is reduced in hypertension. Nat. Commun. *9*, 4878. https://doi.org/10.1038/s41467-018-07318-3.

Nedergaard, M. (2013). Garbage truck of the brain. Science *340*, 1529–1530. https://doi.org/10.1126/science.1240514.Garbage.

Novotny, C., Pötzi, C., Asenbaum, S., Peloschek, P., Suess, E., and Hoffmann, M. (2009). Spect/ct fusion imaging in radionuclide cisternography for localization of liquor leakage sites. J. Neuroimaging *19*, 227–234. https://doi.org/10.1111/j.1552-6569.2008.00270.x.

Oernbo, E.K., Lykke, K., Steffensen, A.B., Töllner, K., Kruuse, C., Rath, M.F., Löscher, W., and MacAulay, N. (2018). Cerebral influx of Na + and Cl - as the osmotherapy-mediated rebound response in rats. Fluids Barriers CNS *15*, 27. https://doi.org/10.1186/s12987-018-0111-8.

Pardridge, W.M. (2005). The blood-brain barrier: bottleneck in brain drug development. NeuroRx *2*, 3–14. https://doi.org/10.1602/neurorx.2.1.3.

Pizzo, M.E., Wolak, D.J., Kumar, N.N., Brunette, E., Brunnquell, C.L., Hannocks, M.J., Abbott, N.J., Meyerand, M.E., Sorokin, L., Stanimirovic, D.B., and Thorne, R.G. (2018). Intrathecal antibody distribution in the rat brain: surface diffusion, perivascular transport and osmotic enhancement of delivery. J. Physiol. *596*, 445–475. https://doi.org/10.1113/JP275105.

Plog, B.A., Mestre, H., Olveda, G.E., Sweeney, A.M., Kenney, H.M., Cove, A., Dholakia, K.Y., Tithof, J., Nevins, T.D., Lundgaard, I., et al. (2018). Transcranial optical imaging reveals a pathway for optimizing the delivery of immunotherapeutics to the brain. JCI Insight *3*, 120922–121015. https://doi.org/10.1172/jci.insight.120922.

Pullen, R.G., DePasquale, M., and Cserr, H.F. (1987). Bulk flow of cerebrospinal fluid into brain in response to acute hyperosmolality. Am. J. Physiol. *253*, F538–F545. https://doi.org/10.1152/ajprenal.1987.253.3.f538.

Rasmussen, M.K., Mestre, H., and Nedergaard, M. (2018). The glymphatic pathway in neurological disorders. Lancet Neurol. *17*, 1016–1024.

Rehling, M., Møller, M.L., Thamdrup, B., Lund, J.O., and Trap-Jensen, J. (1984). Simultaneous measurement of renal clearance and plasma clearance of 99mTc-labelled diethylenetriaminepenta-acetate, 51Cr-labelled ethylenediaminetetra-acetate and inulin in man. Clin. Sci. *66*, 613–619.

Rehling, M., Nielsen, L.E., and Marqversen, J. (2001). Protein binding of 99tcm-dtpa compared with other gfr tracers. Nucl. Med. Commun. *22*, 617–623. https://doi.org/10.1097/00006231-200106000-00003.

Ringstad, G., Valnes, L.M., Dale, A.M., Pripp, A.H., Vatnehol, S.A.S., Emblem, K.E., Mardal, K.A., and Eide, P.K. (2018). Brain-wide glymphatic enhancement and clearance in humans assessed with MRI. JCI Insight *3*, 121537. https://doi.org/10.1172/jci.insight.121537.

Speck, U., Press, W.R., and Mützel, W. (1988). Osmolality-related effects of injections into the central nervous system. Invest. Radiol. *23* (*Suppl 1*), 114–117. https://doi.org/10.1097/00004424-198809001-00013.

Stanton, E.H., Persson, N.D.Å., Gomolka, R.S., Lilius, T., Sigurðsson, B., Lee, H., Xavier, A.L.R., Benveniste, H., Nedergaard, M., and Mori, Y. (2021). Mapping of CSF transport using high spatiotemporal resolution dynamic contrast-enhanced MRI in mice: effect of anesthesia. Magn. Reson. Med. *85*, 3326–3342. https://doi.org/10.1002/mrm.28645.

Taylor, A.T. (2014). Radionuclides in nephrourology, Part 1: radiopharmaceuticals, quality control, and quantitative indices. J. Nucl. Med. *55*, 608–615. https://doi.org/10.2967/jnumed.113.133447.Radionuclides.

Terstappen, G.C., Meyer, A.H., Bell, R.D., and Zhang, W. (2021). Strategies for delivering therapeutics across the blood–brain barrier. Nat. Rev. Drug Discov. *20*, 362–383. https://doi.org/10.1038/s41573-021-00139-y.

Thorne, R.G., and Frey, W.H. (2001). Delivery of neurotrophic factors to the central nervous system. Clin. Pharmacokinet. *40*, 907–946. https://doi.org/10.2165/00003088-200140120-00003.

Todd, M.M. (2013). Hyperosmolar therapy and the brain. Anesthesiology *118*, 777–779. https://doi.org/10.1097/aln.0b013e3182815980.

Tølløfsrud, S., Tønnessen, T., Skraastad, O., and Noddeland, H. (1998). Hypertonic saline and dextran in normovolaemic and hypovolaemic healthy volunteers increases interstitial and intravascular fluid volumes. Acta Anaesthesiol. Scand. *42*, 145–153. https://doi.org/10.1111/j.1399-6576.1998.tb05100.x.

Tustison, N.J., Avants, B.B., Cook, P.A., Zheng, Y., Egan, A., Yushkevich, P.A., and Gee, J.C. (2010). N4ITK: improved N3 bias correction. IEEE Trans. Med. Imag. *29*, 1310–1320. https://doi.org/10.1109/TMI.2010.2046908.

Ullman, J.C., Arguello, A., Getz, J.A., Bhalla, A., Mahon, C.S., Wang, J., Giese, T., Bedard, C., Kim, D.J., Blumenfeld, J.R., et al. (2020). Brain delivery and activity of a lysosomal enzyme using a blood-brain barrier transport vehicle in mice. Sci. Transl. Med. *12*. https://doi.org/10.1126/scitranslmed.aay1359.

Verbalis, J.G. (2010). Brain volume regulation in response to changes in osmolality. Neuroscience *168*, 862–870. https://doi.org/10.1016/j.neuroscience.2010.03.042.

Verma, A., Hesterman, J.Y., Chazen, J.L., Holt, R., Connolly, P., Horky, L., Vallabhajosula, S., and Mozley, P.D. (2020). Intrathecal 99mTc-DTPA imaging of molecular passage from lumbar cerebrospinal fluid to brain and periphery in humans. Alzheimer's and Dementia: Diagnosis, Assessment and Disease Monitoring *12*. https://doi.org/10.1002/dad2.12030.

Xavier, A.L.R., Hauglund, N.L., von Holstein-Rathlou, S., Li, Q., Sanggaard, S., Lou, N., Lundgaard, I., and Nedergaard, M. (2018). Cannula implantation into the cisterna magna of rodents. JoVE, e57378. https://doi.org/10.3791/57378.

Xie, L., Kang, H., Xu, Q., Chen, M.J., Liao, Y., Thiyagarajan, M., O'Donnell, J., Christensen, D.J., Nicholson, C., Iliff, J.J., et al. (2013). Sleep drives metabolite clearance from the adult brain. Science *342*, 373–377. https://doi.org/10.1126/science.1241224.

Yang, L., Kress, B.T., Weber, H.J., Thiyagarajan, M., Wang, B., Deane, R., Benveniste, H., Iliff, J.J., and Nedergaard, M. (2013). Evaluating glymphatic pathway function utilizing clinically relevant intrathecal infusion of CSF tracer. J. Transl. Med. *11*, 107. https://doi.org/10.1186/1479-5876-11-107.

Yushkevich, P.A., Piven, J., Hazlett, H.C., Smith, R.G., Ho, S., Gee, J.C., and Gerig, G. (2006). User-guided 3D active contour segmentation of anatomical structures: significantly improved efficiency and reliability. Neuroimage *31*, 1116–1128. https://doi.org/10.1016/j.neuroimage.2006.01.015.

STAR★METHODS

KEY RESOURCES TABLE

REAGENT or RESOURCE	SOURCE	IDENTIFIER
Chemicals, peptides, and recombinant proteins		
Sodium chloride	Sigma-Aldrich	S3014; CAS: 7647-14-5
Ketamine	MSD	Ketaminol Vet 100 mg/mL
Dexmedetomidine	Orion Pharma	Dexdomitor 0.5 mg/mL
Isoflurane	ScanVet	Attane Vet. 1000 mg/g
Lidocaine	Accord	Lidocain Accord 10 mg/mL
Carprofen	Zoetis	Rimadyl 50 mg/mL
Critical commercial assays		
Technescan DTPA kit	Curium Pharma	Technescan DTPA
Deposited data		
Code for analysis of SPECT/CT data	This paper	https://doi.org/10.6084/m9.figshare.21150415
Code for analysis of MRI data	This paper	https://doi.org/10.6084/m9.figshare.21150415
Code for group-wise activity overlap and subtraction in Figure 1M	This paper	https://doi.org/10.6084/m9.figshare.21150415
Experimental models: Organisms/strains		
Rat: Sprague-Dawley	Janvier	Sprague-Dawley rats
Software and algorithms		
ImageJ	https://imagej.nih.gov/ij/	ImageJ
ITK-SNAP	http://www.itksnap.org/pmwiki/pmwiki.php	ITK-SNAP
GraphPad Prism 7	https://www.graphpad.com/scientific-software/prism/	GraphPad Prism
MILabs Reconstruction software 10.16		N/A
Matlab R2019a	https://se.mathworks.com/products/matlab.html	Matlab
Noldus EthoVision XT 10	https://www.noldus.com/ethovision-xt	EthoVision XT
Paravision Bruker v6.0.1	https://www.bruker.com/en/products-and-solutions/preclinical-imaging/paravision-360.html	N/A
Advanced Normalization Tools v2.3.4	https://sourceforge.net/projects/advants/	N/A

RESOURCE AVAILABILITY

Lead contact

Further information and requests for resources and reagents should be directed to the lead contact, Maiken Nedergaard (maiken_nedergaard@urmc.rochester.edu).

Materials availability

This study did not generate new unique reagents.

Data and code availability

- All data reported in this paper will be shared by the lead contact on request.
- Original code used in the analysis of SPECT/CT and MRI data, and for visualization of group-wised averaged activity in Figure 1M has been deposited at Figshare and is publicly available as of the date of publication. DOIs are listed in the key resources table.

- Any additional information required to reanalyze the data reported in this paper is available from the lead contact upon request.

EXPERIMENTAL MODEL AND SUBJECT DETAILS

Animals

All the animal procedures were approved by the Danish Animal Experiments Inspectorate under the Danish Ministry of Environment and Food, license 2015-15-0201-00535, apart from the behavioral experiments, which were approved by the County Administrative Board of Southern Finland, license ESAVI/9697/04.10.07/2017. Female Sprague-Dawley rats (10-13 weeks, 175–250 g) acquired from Janvier were used in the experiments. Rats were group-housed in 12:12h light cycle with access to food and water *ad libitum*. All efforts were made to minimize pain or discomfort of the animals used. The well-being of the animals was monitored daily, indicated by grooming behavior and body posture. After implantation of a guide cannula in the experiments that involved striatal infusions, the rats were moved to single housing overnight to prevent detachment of the cannula. All experiments were performed at Zeitgeber time 2-10.

METHOD DETAILS

Tracers

To visualize the effects of HTS on glymphatic transport, clinical grade ^{99m}Tc-labeled diethylenetriamine-pentaacetic acid (12.5 mg/mL, TechneScan DTPA, Curium Pharma; MW 489 Da) was used as a radiotracer for dynamic SPECT/CT imaging. For intracisternal and intrastriatal administration, the tracer was infused with a Hamilton Gastight 1700 syringe in a micro infusion pump (cisternal: 32 μL, 1.6 μL/min, 10–60 MBq; striatal: 4 μL, 0.2 μL/min, 3–7 MBq). Intravenously administered tracer was delivered as bolus dose (200 μL, 20–40 MBq). Radioactivity concentration of the infused dose was measured with a VIK-202 dose calibrator (Comecer).

Treatments

The animals received either isotonic saline (ITS, 0.154 M NaCl in ddH_2O, 6.16 mOsm/kg, control group) or hypertonic saline (HTS, 1 M NaCl in ddH_2O) intraperitoneally (20 mL/kg, 40 mOsm/kg; over one minute).

Tracer administration routes

Intracisternal

The animals were anesthetized with ketamine (100 mg/kg) and dexmedetomidine (0.5 mg/kg) administered together subcutaneously (2 mL/kg) and, after a loss of toe-pinch reflex, were fixed to a stereotaxic frame with the head slightly tilted forward (30°). The intracisternal cannula was placed as previously described, with minor modifications (Xavier et al., 2018). In brief, the atlanto-occipital membrane overlying the cisterna magna (CM) was surgically exposed and a cannula consisting of a 30G short-beveled dental needle attached to PE10 tubing was carefully inserted into the intrathecal space, while avoiding any CSF leakage outside CM. The cannula was fixed to the dura with cyanoacrylate glue and dental cement. The animals were transferred to SPECT/CT imaging system immediately after cannula installation.

Intrastriatal

The intrastriatal cannulae were surgically placed on the day before the SPECT experiment. The animals were anesthetized with isoflurane (3.5–4% induction, 1.5–2% maintenance in 100% O_2) and, after a loss of tail-pinch reflex, were fixed to a stereotaxic frame. At the beginning of the surgery, lidocaine (1 mg/kg) was administered as a local anesthetic, while carprofen (5 mg/kg, s.c.) was administered as a postoperative analgesic. A small burr hole was drilled in the skull over the striatum of the right cerebral hemisphere and a guide cannula was inserted in the striatum (M/L: 3.0 mm; A/P: 0.0 mm; D/V: −5.0 mm) and fixed to the skull with cyanoacrylate glue and dental cement. The rats were allowed to recover for 16–24 h in single-housing before SPECT/CT imaging.

Intravenous

The animals were anesthetized with a ketamine (100 mg/kg) and dexmedetomidine (0.5 mg/kg) administered together subcutaneously (2 mL/kg). The tail vein was dilated by submerging the tail in warm water. After a loss of tail-pinch reflex, a 24G intravenous cannula (BD Neoflon) was inserted in the tail vein and

fixed in place with surgical tape. The animals were transferred to SPECT/CT imaging system immediately after cannula installation.

SPECT/CT-imaging

For the duration of the scans, rats in all groups were anesthetized with a mixture of ketamine (100 mg/kg) and dexmedetomidine (0.5 mg/kg) administered together subcutaneously (2 mL/kg). The respiratory rate was monitored with a pressure pad to ensure a sufficient level of anesthesia. No supplemental anesthesia was needed in any of the scans. A 24G venous cannula (BD Neoflon) was inserted into the intraperitoneal cavity of the rats and glued on the skin for HTS/ITS administration. Dynamic whole-body SPECT/CT imaging was performed with the Vector4CT (MILabs, Utrecht, Netherlands) system. Rats were randomized to either ITS or HTS group and placed in the scanner in the prone position. SPECT images were acquired with a high energy ultra-high-resolution rat 1.8 mm pinhole collimator (HE-UHR-RM 1.8 mm diameter). Image data were acquired over 220 min (twenty-two 10-min scans). The rectal temperature of the animal was monitored throughout the entire scan and normothermia was maintained with a thermostatically regulated heating pad. The SPECT image was registered to whole-body CT images acquired directly after the SPECT scans that served as anatomical reference images.

SPECT/CT analysis

Acquired images were reconstructed using Similarity-Regulated Ordered Subsets Estimation Maximization (SROSEM) with a voxel size of 300 μm and five iterations with correction for attenuation and tracer decay in MILabs Reconstruction software 10.16 (MILabs, Utrecht, Netherlands). Regions of interest (ROIs) were defined in ITK-SNAP software (Yushkevich et al., 2006) with a combination of manual and automated segmentation using the acquired SPECT and CT images. The CNS ROIs included intracranial space, spine, and spherical volumes of interest (VOIs) placed in different brain structures (striatum, cortex, hippocampus, ventricles, and olfactory bulbs) using an in-house template (Figure S2I). ROIs relevant to CSF clearance routes included nasal cavity, mandibular lymph nodes (MLN), deep cervical lymph nodes (DCLN), left and right kidney, and urine, which consisted of the bladder contents and the surgical pad placed underneath the animal for urine collection. A heart ROI was segmented to represent the blood compartment. The total injected activity was determined as the activity calculated in the whole animal – including urine pad, but excluding the infusion cannula – in the first frame after the end of the tracer infusion. The fraction of the total activity in the injected dose (%ID) in each ROI was calculated from the acquired SPECT images using MATLAB R2019a (Mathworks). Soft tissue regions that were not clearly outlined in CT images, including lymph nodes, kidneys, and heart were normalized to the volume of the corresponding ROI.

Behavioral tests

Open field test

The open field test was used to measure the effects of HTS on locomotor activity and exploratory behavior of the animals. The rats were released in the corner of a transparent open field arena (50 × 50 cm, white floor, Med Associates). Horizontal and vertical activities were recorded during a 30-min trial (light intensity ~100 lx) beginning immediately after or 24 h after treatment administrations. The infrared photobeam interruptions were registered at 5-min intervals. A peripheral zone was defined as a 7.5 cm wide corridor along the wall to define by exclusion the time spent in the central area of the arena.

Elevated plus maze

The elevated plus maze (EPM) was used to measure anxiety-like behavior of the rats. The EPM consisted of two open arms (50 × 10 cm) and two enclosed arms (50 × 10 × 30 cm) connected by a central platform (10 × 10 cm). The maze configuration formed the shape of a plus sign, with the two open arms opposite to each other. The maze was raised to 80 cm above floor level. The rat was placed on the central platform immediately after treatment administration, always facing the same enclosed arm, and its behavior was video tracked for five minutes. Time spent in the open and closed arms and the distance traveled were quantified using the Noldus EthoVision XT 10 system (Noldus Information Technology).

Rotarod

To measure the effects of HTS on motor coordination, the accelerating Rotarod (Ugo Basile, Comerio, Italy) test was performed four times in succession: 15, 30, 60 and 120 min after treatment administrations. The rats received three days of training on the Rotarod before the experiment. For the training, the cylinder

(diameter 6 cm) rotated at constant speed of 10 rpm and the animals were placed on the rod for 60 s. For the testing, the cylinder rotated at 10 rpm and accelerated to 40 rpm over the duration of 60 s. A cut-off time of 60 s was chosen for each test.

MR imaging

The anesthetic regimen, physiological monitoring, and placement of HTS cannula was performed much as described above for SPECT/CT imaging. MR images were acquired on a Bruker BioSpec 94/30 USR magnet interfaced to a Bruker Advance III console, controlled by Paravision software (Bruker v6.0.1). Imaging was carried out using an 86 mm volume RF-transmit coil and a 4-channel phased array RF-receive coil (Bruker). Imaging sequences consisted of T2-weighted TurboRARE (TE: 24.1 ms, TR: 16 s, Echo spacing: 8.033, RARE factor: 8, matrix: 375 × 250, FOV 30 × 20 mm, in-plane resolution: 0.08 × 0.08 mm, 128 slices, 220 μm slice thickness, 110 μm overlap, scan time per repetition: 6 min and 8 s). 8 frames (50 min) were acquired at baseline and 12 frames (72 min) after HTS infusion, for a total of 20 frames.

MRI analysis

T2-weighted images were corrected for motion (Advanced Normalization Tools, v2.3.4), followed by performance of bias field correction as follows: First, in-house software was used to remove a second-order bias field in the ventral-dorsal direction arising from the use of a surface receiver coil. Second, local bias fields were corrected using N4 (Tustison et al., 2010). The first eight frames and last eight frames, respectively, were averaged to create pre- and post-HTS images. The four frames following HTS infusion constituted the transition period and were thus discarded. Pre- and post-HTS images were then segmented into brain tissue and CSF as follows: ROIs representative of white matter, gray matter and CSF were drawn manually using ITK-SNAP software. Probability maps for each tissue type were then calculated for pre- and post-HTS respectively, assuming a normal intensity distribution within each tissue type, with means and variances calculated from the representative ROIs. Each pixel in the brain was then labeled as the highest probability tissue type, whereupon white and gray matter labels were merged.

Osmolality and sodium measurements

A separate set of animals were decapitated 30 min or two hours after HTS/ITS administrations, and their trunk blood was collected in EDTA tubes. The blood samples were centrifuged, and the separated plasma was collected. Other set of animals were anesthetized with a mixture of ketamine (100 mg/kg) and dexmedetomidine (0.5 mg/kg) administered together subcutaneously (2 mL/kg) 30 min or two hours after HTS/ITS administrations, and CSF samples were collected via a cannula placed in the CM in a similar manner as before intracisternal tracer administrations. The osmolalities of the plasma and CSF samples were measured by the freezing-point method using a Type 15 Micro-Osmometer (Löser Meßtechnik). Sodium concentration of the plasma samples were determined with ion-selective electrode-based method using an ARCHITECT c8000 analyzer (Abbott Diagnostics).

QUANTIFICATION AND STATISTICAL ANALYSIS

All statistical testing was performed using GraphPad Prism 7 (GraphPad Software). For SPECT/CT tracer distribution analysis, area under curve ($AUC_{0\text{-}220}$) was determined from time-activity plots of individual animals and ROIs and the results were compared group-wise with unpaired Student's t-test. In behavioral tests, unpaired Student's t-test was used to compare the behavioral effects between treatment groups. All statistical tests were two-tailed. Details of each statistical test are described in the figure legend. p-value of less than 0.05 was considered statistically significant.